16th World Conference on Earthquake Engineering, 16WCEE 2017
Santiago Chile, January 9th to 13th 2017
Paper N° 3728 (Abstract ID)
Registration Code: S-D1464689697

RISK-INFORMED OPTIMIZATION OF THE TUNED MASS-DAMPER-INERTER (TMDI) FOR SEISMIC PROTECTION OF BUILDINGS IN CHILE

R. Ruiz[(1)], A. Giaralis[(2)], A. Taflanidis[(3)], D. Lopez-Garcia[(4),(5)]

[(1)] *Post Doctoral researcher, University of Chile, rruizgarcia@ing.uchile.cl*
[(2)] *Senior Lecturer, City University London, agathoklis@city.ac.uk*
[(3)] *Associate Professor, University of Notre Dame, a.taflanidis@nd.edu*
[(4)] *Associate Professor, Pontificia Universidad Catolica de Chile, dlg@ing.puc.cl*
[(5)] *Researcher, National Research Center for Integrated Natural Disaster Management CONICYT/FONDAP/15110017, dlg@ing.puc.cl*

Abstract

In recent decades, the concept of the passive linear tuned mass-damper (TMD) has been considered as a valid option for vibration suppression of dynamically excited building structures due to its relatively simple design and practical implementation. Conceptually, the TMD comprises a mass attached to the structure whose vibration motion is to be controlled (primary structure) via optimally designed/"tuned" linear spring and viscous damper elements. Aside from the dynamical properties of the primary structure, the effectiveness of the TMD depends heavily on the inertia of the attached mass and on the attributes and nature of the dynamic excitation. For effective control of wind-induced vibrations a TMD mass weighting in between 0.5% to 1% of the total building weight is usually sufficient. However, controlling earthquake induced oscillations in buildings commonly requires a significantly heavier TMD mass. In this respect, recently, a generalization of the passive linear TMD was proposed incorporating an "inerter" device: the tuned mass-damper-inerter (TMDI). The inerter is a two-terminal device developing a resisting force proportional to the relative acceleration of its terminals. The underlying constant of proportionality (inertance) can be up to two orders of magnitude larger than the device physical mass. In this regard, it was shown analytically and numerically that optimally designed TMDI outperforms the classical TMD for a fixed attached mass in terms of relative displacement variance of linear primary structures under stochastic seismic excitations by exploiting the "mass amplification" inerter property.

In this work, the optimal risk-informed design of the TMDI for seismic protection of multi-storey buildings in the region of Chile is addressed. Note that the Chilean seismo-tectonic environment is dominated by large magnitude seismic events yielding ground motions of long effective duration whose damage potential can be well reduced by means of TMDs. In this respect, a probabilistic framework is established for design optimization considering seismic risk criteria. Quantification of this risk through response analysis is considered and the seismic hazard is described by a recently developed stochastic ground motion model that offers hazard-compatibility with ground motion prediction equations available for Chile. Multiple criteria are utilized in the design optimization. The main one, representing overall direct benefits, is the life-cycle cost of the system, composed of the upfront TMDI cost and the anticipated seismic losses over the lifetime of the structure. For enhanced decision support, two additional criteria are examined, both represented through some response characteristic with specific probability of exceedance over the lifetime of the structure (therefore corresponding to design events with specific annual rate of exceedance). One such characteristic corresponds to the repair cost, and incorporates risk-averse attitudes into the design process, whereas the other corresponds to the inerter force, which incorporates practical constraints for the force transfer between TMDI and the supporting structure. This ultimately leads to a multi-objective formulation of the design problem. Stochastic simulation is used to estimate all required risk measures, whereas a Kriging metamodel is developed to support an efficient optimization process. The results show that the proposed design framework facilitates a clear demonstration of the benefits of the TMDI (over the TMD) as well as the evaluation of the comparative benefits of increasing the mass of the TMD against increasing the inertance of the TMDI.

Keywords: tuned mass damper, inerter, multi-objective design, risk based design, risk aversion, Chile

1. Introduction

The tuned mass damper (TMD) is arguably the most commonly considered passive dynamic vibration absorber for the seismic protection of building structures [1-4]. In its classical form, it consists of a mass attached towards the top of the building whose earthquake-induced vibration motion is to be suppressed (primary structure) via optimally designed/"tuned" linear spring and dashpot elements. Through appropriate tuning of the TMD dynamic characteristics the attached mass counteracts the motion of the primary structure [5]. In this manner, the kinetic energy of the primary structure is transferred to the attached mass and is eventually dissipated at the dashpot. Although closed-form expressions for optimally tuned TMD properties do exist (e.g., [6]), numerical optimization approaches are commonly employed in TMD design. No matter what design approach is adopted, the inertial property of the TMD becomes a critical parameter in establishing satisfactory performance for seismic applications [7-9]: the larger the attached TMD mass that can be accommodated, subject to structural design and architectural constraints, the more effective the TMD will be. In this regard, several researchers examined the seismic performance achieved under unconventionally large TMDs, including approaches to accommodate such large attached/secondary masses [10-12].

Recently, a generalization of the classical TMD, termed tuned mass-damper-inerter (TMDI), was proposed by Marian and Giaralis [13, 14] to enhance the TMD vibration suppression performance without any significant increase to the attached mass/weight. This is achieved by coupling the TMD with an inerter: a two-terminal mechanical device developing a resisting force proportional to the relative acceleration of its terminals [15]. The underlying constant of proportionality ("inertance") can be orders of magnitude larger than the physical mass of the inerter. Therefore, the TMDI, shown in Fig.1 for a multi-storey building primary structure, can potentially outperform the classical TMD for the same attached mass, if properly tuned/designed, by relying on the "mass amplification" property of the inerter. In fact, it was shown in [13, 14] that optimally designed TMDIs with relatively small attached mass installed on the top floor of linear shear frame structures outperform the classical TMD in minimizing the top floor displacement variance under Eurocode 8 response spectrum compatible stochastic seismic excitation. Moreover, Giaralis and Taflanidis [16] employed a reliability-based optimum design approach to study the effectiveness of several different TMDI topologies for vibration suppression in linear multi-storey building structures excited by stochastic seismic excitation, while Giaralis and Marian [17] demonstrated that the TMDI achieves the same seismic performance level for significantly smaller attached mass compared to the classical TMD.

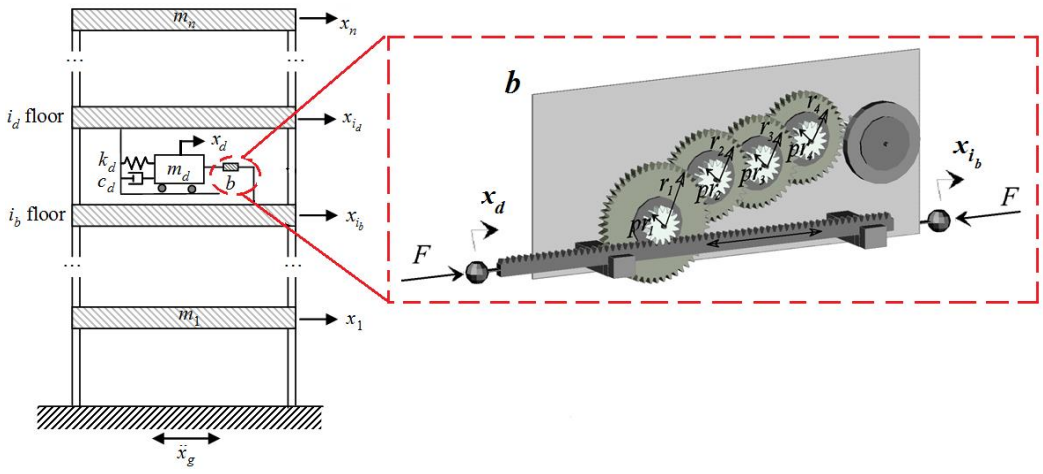

Fig. 1– Tuned mass-damper-inerter (TMDI) equipped multi-storey frame structure and schematic representation of a rack-and-pinion flywheel-based inerter device with 4 gearing stages

In all the above studies on the TMDI only shear frame building structures have been adopted in assessing the effectiveness of the TMDI without any particular site-specific seismic hazard considerations. Furthermore, TMDI optimization was based solely on structural response criteria, without any risk-related considerations or

cost-benefit analysis. In this regard, this paper focuses on the optimal risk-informed design of the TMDI accounting for life-cycle monetary cost for the seismic protection of multi-storey buildings in the region of Chile by considering an existing 21-storey building structure as a case-study. The work is motivated by the fact that TMDs are particularly efficient in reducing structural damage potential of earthquakes generated in the Chilean seismo-tectonic environment [18], which is dominated by large magnitude seismic events yielding ground motions of long effective duration. The herein study extends the research efforts in [18] by utilizing risk-related design concepts to explore the potential benefits of the TMDI vis-à-vis the conventional TMD in addressing the problem at hand in a cost-efficient manner. Risk quantification is accomplished through linear response history analysis, whereas the seismic hazard is described through a stochastic ground motion model that offers hazard-compatibility with ground motion prediction equations available for Chile. Multiple criteria are utilized in the design optimization. The main one, representing overall direct benefits, is the life-cycle cost of the system, composed of the upfront TMDI cost and the anticipated seismic losses over the lifetime of the structure. For enhanced decision support, two additional criteria are examined, both represented though some response characteristic with specific probability of exceedance over the lifetime of the structure (therefore corresponding to design events with specific annual rate of exceedance). One such characteristic corresponds to the repair cost, and incorporates risk-averse attitudes into the design process, whereas the other corresponds to the inerter force, which incorporates practical constraints for the force transfer between TMDI and the supporting structure. This ultimately leads to a multi-objective formulation of the design problem. Stochastic simulation is used to estimate all risk measures, whereas a Kriging metamodel is developed to support an efficient optimization process.

The remaining of the paper is organized as follows. In the next Section the equations of motion of the TMDI are reviewed, followed (Section 3) by the probabilistic framework for the performance quantification. In Section 4 the multi-objective design is discussed, including numerical details for its implementation. Section 5 furnishes pertinent numerical data for a real-life existing building in Santiago, Chile to demonstrate the benefits of the TMDI (over the TMD) within the proposed design framework, while Section 6 summarizes conclusions.

2. Equations of motion of TMDI equipped multi-storey frame buildings

2.1 The ideal linear inerter

The ideal inerter, conceptually introduced by Smith [15], is a linear two terminal device of negligible mass/weight developing a resisting force proportional to the relative acceleration of its terminals which are free to move independently. As an example, the internal force of the inerter shown in Fig. 1 is given by

$$F = b(\ddot{x}_d - \ddot{x}_{i_b}), \tag{1}$$

where x_d and x_{ib} are the displacement coordinates of the inerter terminals and, hereafter, a dot over a symbol signifies time differentiation. In the above equation, the constant of proportionality b is the so-called inertance and has mass units. Importantly, the physical mass of actual inerter devices can be two or more orders of magnitude lower than b. This has been experimentally validated by testing several flywheel-based prototyped inerter devices incorporating rack-and-pinion or ball-screw mechanisms to transform the translational kinetic energy into rotational kinetic energy "stored" in a relatively light rotating disk (flywheel) [19]. More recently, fluid/hydraulic-based inerters achieving inertance values b that are almost independent of the physical device mass were also been built and tested [20, 21].

To elaborate further on this point, consider a typical realisation of the inerter comprising a flywheel linked to a rack-and-pinion via n gears (Fig. 1 depicts such a device for n=4). The inertance of this device is given by

$$b = m_f \frac{\gamma_f^2}{\gamma_{pr}^2} \left(\prod_{k=1}^{n} \frac{r_k^2}{pr_k^2} \right) \tag{2}$$

where m_f and γ_f are the mass and the radius of gyration of the flywheel (right-most circular solid disk shown in Fig.1), respectively, γ_{pr} is the radius of the flywheel pinion, and r_k and pr_k (k=1,2,..,n) are the radii of the k-th gear and its corresponding pinion, respectively, linking the rack to the flywheel pinion. Assuming a flywheel of

10kg mass with a ratio γ_f/γ_{pr}= 3 driven by a single gear (i.e., n=1) with a r_1/pr_1=4 gear ratio, the inertance computed from Eq. (2) is b= 1440kg (see also [15]). Adding two more gears with a common gear ratio equal to 3, yields an inerter with b= 116640kg, that is, a device with a physical mass three orders of magnitude smaller than its inertance. Although inerters at the scale of civil engineering structures are not commercially available yet (inerters are currently used only in automotive industry applications), the above simple example illustrates the scalability of flywheel-based inerters through gearing, as well as the affordability in manufacturing. Importantly, in view of (1) and (2), the inerter can be seen as a mass amplification device from the structural dynamics viewpoint, since by fixing any one terminal, the device acts as a "weightless" mass b. This observation motivated the consideration of the tuned mass-damper-inerter, reviewed in the next sub-section.

2.2 Equations of motion for an inerter equipped frame structure

Consider the planar n-storey frame building, shown in Fig. 1, whose oscillatory motion due to a ground acceleration $\ddot{x}_g$ is to be suppressed (primary structure). The TMDI consists of a classical linear passive tuned mass-damper (TMD) located at the i_d-th floor of the primary structure comprising a mass m_d attached to the structure via a linear spring of stiffness k_d and a linear dashpot of damping coefficient c_d. The TMD mass is linked to the i_b-th floor by an inerter with inertance b. Practical considerations suggest that i_d corresponds to the top floor and i_b to one floor below. However, the following formulation allows for different TMDI topologies.

Let $\mathbf{x}_s \in \mathbb{R}^n$ be the vector of floor displacements of the primary structure relative to the ground and $\ddot{x}_g \in \mathbb{R}$ be the ground acceleration. Denote by $\mathbf{R}_d \in \mathbb{R}^n$ the *TMD location* vector specifying the floor the TMD is attached to (i.e., vector of zeros with a single one in its i_d entry), and by $\mathbf{R}_b \in \mathbb{R}^n$ be the *inerter location* vector specifying the floor the inerter is connected to (i.e., vector of zeros with a single one in its i_b entry). Let, also, $y \in \mathbb{R}$ be the displacement of the TMD mass relative to the i_d floor and define the *connectivity* vector by $\mathbf{R}_c$=$\mathbf{R}_d$-$\mathbf{R}_b$. Then, the resisting force developing within the inerter in (1) is equal to $b(\mathbf{R}_c\ddot{x}_s + \ddot{y})$ and the coupled equations of motion for the TMDI equipped primary structure in Fig.1 modeled as lumped-mass damped multi degree-of-freedom (MDOF) system are written as

$$\left(\mathbf{M}_s + \mathbf{R}_d m_d \mathbf{R}_d^T + \mathbf{R}_c b \mathbf{R}_c^T\right)\ddot{\mathbf{x}}_s(t) + \left(m_d \mathbf{R}_d + b\mathbf{R}_c\right)\ddot{y}(t) + \mathbf{C}_s\dot{\mathbf{x}}_s(t) + \mathbf{K}_s\mathbf{x}_s(t) = -\left(\mathbf{M}_s + \mathbf{R}_d m_d \mathbf{R}_d^T\right)\mathbf{R}_s\ddot{x}_g(t) \quad (3)$$

$$(m_d + b)\ddot{y}(t) + \left(m_d\mathbf{R}_d^T + b\mathbf{R}_c^T\right)\ddot{\mathbf{x}}_s(t) + c_d\dot{y}(t) + k_d y(t) = -m_d\mathbf{R}_d^T\mathbf{R}_s\ddot{x}_g(t) \quad (4)$$

In (3), $\mathbf{M}_s \in \mathbb{R}^{nxn}$, $\mathbf{C}_s \in \mathbb{R}^{nxn}$, and $\mathbf{K}_s \in \mathbb{R}^{nxn}$ are the mass, damping, and stiffness matrices of the primary structure, respectively, and $\mathbf{R}_s \in \mathbb{R}^n$ is the earthquake influence coefficient vector (vector of ones). Note that in deriving (3) and (4) the inerter is taken as weightless, and, therefore, it does not attract any seismic lateral force [14]. Equation (4) suggests that the total inertia of the TMDI is equal to (m_d+b). Hence, the TMDI frequency ratio f_d, damping ratio ζ_d, inertance ratio β, and mass ratio μ are defined as

$$f_d = \sqrt{\frac{k_d}{(m_d + b)}} / \omega_1; \quad \zeta_d = \frac{c_d}{2(m_d + b)\omega_d}; \quad \beta = \frac{b}{M}; \quad \mu = \frac{m_d}{M} \quad (5)$$

where ω_1 and M is the fundamental natural frequency and the total mass of the primary structure, respectively. The inerter force, explicitly utilized in the design framework developed next, is $F_i(t) = b\left[\ddot{y}(t) + \mathbf{R}_c\ddot{\mathbf{x}}_s(t)\right]$.

3. Quantification of risk metrics

3.1 Characterization of seismic risk

The quantification of seismic risk follows the framework initially discussed in [22] (also shown in Fig. 2). It relies on adopting appropriate models for the seismic excitation (hazard analysis), structural system (structural analysis) and loss evaluation (damage and loss analysis), and on assigning appropriate probability distributions to the parameters that are considered as uncertain in these different models. The latter uncertainty characterization supports ultimately the seismic risk quantification. Structural behavior is evaluated through time-history analysis and seismic consequences through an assembly-based vulnerability approach [23], whereas for providing an appropriate within this context description of the seismic excitation (acceleration time-histories)

a site-based stochastic ground motion model is adopted. This model is established by modulating a white noise sequence through functions that address the frequency and time-domain characteristics of the excitation. The parameters of these functions are related to seismological characteristics, the moment magnitude M and the rupture distance r_{rup}, through predictive relationships. Following the approach in [24] these predictive relationships are optimized to provide a regional hazard compatibility by establishing a match to regional ground motion prediction equations [25]. Details about the optimized model may be found in [18]. Once the stochastic ground motion model is optimized the adoption of probability distributions for the seismological parameters facilitates a comprehensive probabilistic description of the seismic hazard [26].

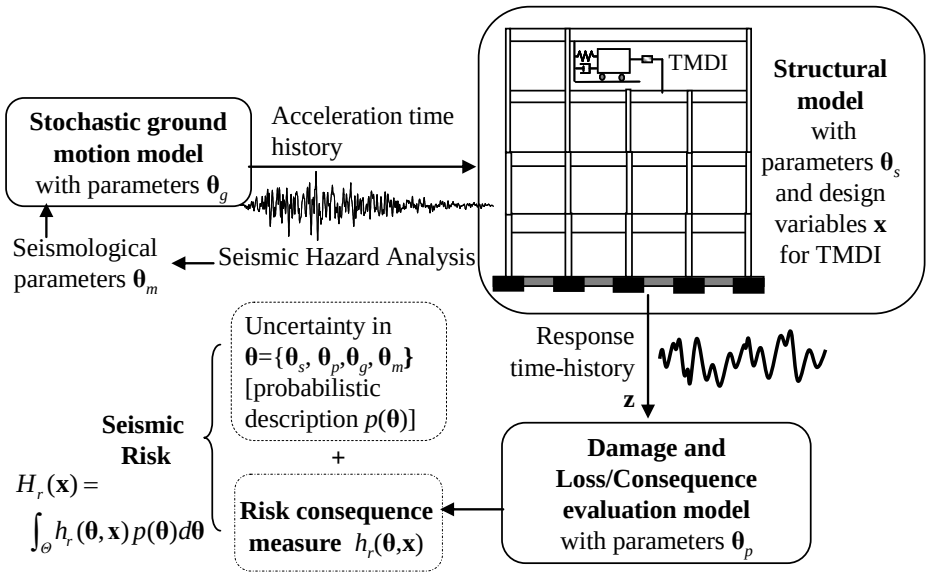

Fig. 2 – Schematic for risk quantification framework

In this context, let $\boldsymbol{\theta}$ lying in $\Theta \subset \Re^{n_\theta}$, be the augmented vector of continuous uncertain model parameters with probability density functions (PDFs) denoted as $p(\boldsymbol{\theta})$, where Θ denotes is space of possible parameter-values. This vector includes all the different parameters (both seismological and structural) that are considered as uncertain as well as the white noise sequence utilized in the ground motion model. Also, let the vector of controllable parameters for the TMDI referred to herein as *design variables*, be $\mathbf{x} \in X \subset \Re^{n_x}$, where X denotes the admissible design space. Ultimately $\mathbf{x}$ includes the mass m_d (or mass ratio μ), the inertance b (or inertance ratio β), the stiffness k_d (or frequency ratio f_d), and the damping coefficient c_d (or damping ratio ζ_d). For a specific design configuration $\mathbf{x}$, the risk consequence measure describing the favorability of the response from a decision-theoretic viewpoint is given by $h_r(\boldsymbol{\theta},\mathbf{x})$. Each consequence measure $h_r(.)$ is related to (i) the earthquake performance/losses that can be calculated based on the estimated response of the structure $\mathbf{z}$ (performance given that some seismic event has occurred), as well as to (ii) assumptions made about the rate of occurrence of earthquakes (incorporation of the probability of seismic events occurring). Seismic risk, $H_r(\mathbf{x})$, is then described through the expected value of the risk-consequence measure, given by the generic multi-dimensional integral

$$H_r(\mathbf{x}) = \int_\Theta h_r(\boldsymbol{\theta},\mathbf{x})\, p(\boldsymbol{\theta}) d\boldsymbol{\theta} \tag{6}$$

Through different selection of the risk consequence measure different risk quantifications can be addressed within this framework, supporting the estimation of all necessary design metrics.

3.2 Design metrics quantification

The main metric utilized in the design formulation is the total life-cycle cost $C(\mathbf{x})=C_i(\mathbf{x})+C_l(\mathbf{x})$, provided by adding the initial (upfront) cost $C_i(\mathbf{x})$, which is a function of the TMDI characteristics, and the cost due to earthquake losses over the life-cycle of the structure $C_l(\mathbf{x})$. For a Poisson assumption for occurrence of earthquakes, as considered in the case study, the present value $C_l(\mathbf{x})$ of expected future seismic losses is given by integral (6) with associated risk consequence measure definition [27]

$$h_r(\boldsymbol{\theta},\mathbf{x}) = C_r(\boldsymbol{\theta},\mathbf{x}) v t_{life}\left[(1-e^{-r_d t_{life}})/(r_d t_{life})\right] \quad (7)$$

where r_d is the discount rate, t_{life} is the life cycle considered and $C_r(\boldsymbol{\theta},\mathbf{x})$ is the cost given the occurrence of an earthquake event. For estimating the latter an assembly-based vulnerability approach is adopted as discussed earlier. According to this approach the components of the structure are grouped into damageable assemblies, which consist of components of the system that have common vulnerability and repair cost characteristics (e.g. ceiling, wall partitions, etc.). Different damage states are designated to each assembly and a fragility function (quantifying the probability that a component has reached or exceeded its damage state) and repair cost estimates are established for each damage state. The former is conditional on some engineering demand parameter (*EDP*), which is related to peak characteristics for the structural response (e.g. peak interstory drift, peak floor acceleration, etc.). Combination of the fragility and cost information provides then $C_r(\boldsymbol{\theta},\mathbf{x})$.

Consideration of only the life-cycle cost as performance objective facilitates what is commonly referenced as "*risk-neutral"* design, which assumes that preference is assessed only through quantities that can be monetized. Frequently nontechnical factors, such as social risk perceptions, need to be taken into account that lead to more conservative designs (*risk aversion*), since *risk-neutral* design does not explicitly address the unlikely but potentially devastating losses that lie on the tail of the losses/consequence distribution. Motivated by this realization the incorporation of an additional performance objective corresponding to repair cost with specific probability of exceedance over the life-cycle of the structure was proposed in [28]. This is adopted here as an additional design metric. Based on the Poisson assumption of seismic events, the probability of the repair cost C_r exceeding a targeted threshold $C_{thresh}(\mathbf{x})$ over the considered lifetime of the structure is

$$P[\mathrm{C}_r > C_{thresh}(\mathbf{x}) \,|\, \mathbf{x}, t_{life}] = 1 - \exp^{-t_{life}\nu \cdot P[\mathrm{C}_r > C_{thresh}(\mathbf{x})|\mathbf{x},\ \text{seismic event}]} \quad (8)$$

where $P[\mathrm{C}_r > C_{thresh}(\mathbf{x}) \,|\, \mathbf{x},\ \text{seismic event}]$ is the probability of exceeding the repair threshold given that a seismic event has occurred. The latter is given by the generic risk integral (6) with risk consequence measure

$$h_r(\boldsymbol{\theta},\mathbf{x}) = I_C(\boldsymbol{\theta},\mathbf{x}) \quad (9)$$

corresponding to an indicator function, being one if $C_r(\boldsymbol{\theta}, \mathbf{x}) > C_{thresh}(\mathbf{x})$ and zero if not.

None of the above two metrics looks explicitly, though, at the strengthening that would be needed to support the transfer of forces from the TMDI to the structural frame. The optimal TMDI configuration typically corresponds to large inertance values [16, 17], which may lead to large values for the inerter force in (1). Accommodation of these forces might require some local strengthening of the structural elements supporting the TMDI. This could be taken into account as a component of the upfront cost $C_i(\mathbf{x})$, though this requires detailed evaluation of alternative retrofitting solutions. Instead, an approximation is established here by adopting as an additional design metric a reference inerter force, corresponding to the force for a specific design event. This is similar to the approach adopted for quantifying the reference capacity for other type of protective devices, such as fluid viscous dampers [29]. This reference force ultimately represents the degree of seismic strengthening that will be required. The design event is quantified here by equivalently looking at the inerter force with specific probability of exceedance over the life-cycle of the structure $P[F_i > F_{thresh}(\mathbf{x}) \,|\, \mathbf{x}, t_{life}]$. This probability is given by an equation similar to (8), simply with risk consequence measure in (9) (used to calculate $P[F_i > F_{thresh}(\mathbf{x}) \,|\, \mathbf{x},\ \text{seismic event}]$) $h_r(\boldsymbol{\theta},\mathbf{x}) = I_i(\boldsymbol{\theta},\mathbf{x})$, being one if $F_i(\boldsymbol{\theta}, \mathbf{x}) > F_{thresh}(\mathbf{x})$ and zero if not.

4. Multi-objective design

4.1 Problem formulation

The multi-criteria design is expressed ultimately as

$$\begin{aligned} \mathbf{x}^* &= \arg\min_{\mathbf{x}\in X} \left\{ C(\mathbf{x}) = C_i(\mathbf{x}) + C_l(\mathbf{x}), C_{thresh}(\mathbf{x}), F_{thresh}(\mathbf{x}) \right\}^T \\ \text{such that } & P[C_r > C_{thresh}(\mathbf{x}) \,|\, \mathbf{x}, t_{life}] = p_{or} \\ & P[F_i > F_{thresh}(\mathbf{x}) \,|\, \mathbf{x}, t_{life}] = p_{oi} \end{aligned} \quad (10)$$

where $C(\mathbf{x})$ [first objective] is the life-cycle cost, $C_{thresh}(\mathbf{x})$ [second objective] is the repair threshold with probability of being exceeded p_{or} over the lifetime of the structure and $F_{thresh}(\mathbf{x})$ [third objective] is the inerter force with probability of being exceeded p_{oi} over the lifetime of the structure. This multi-objective formulation leads ultimately to a set of points (also known as dominant designs) that lie on the boundary of the feasible objective space and they form a manifold: the Pareto front. A point belongs to the Pareto front and it is called Pareto optimal point if there is no other point that improves one objective without detriment to any other. The multi-objective problem allows for the identification of a range of TMDI configurations (Pareto optimal solutions) striking a trade-off among (i) total cost [$C(\mathbf{x})$], (ii) consequences of rare events [$C_{thresh}(\mathbf{x})$] and (iii) strengthening required for facilitating the TMDI force transfer. The first objective is estimated within a life-cycle setting whereas the other two as values corresponding to a design event (specific annual rate of exceedance, defined through p_{or} and p_{oi}). The designer or decision maker (e.g. building owner) can ultimately make the final decision among the Pareto optimal solutions, incorporating any additional considerations including architectural constraints for the TMDI implementation (accommodation of larger TMDI mass).

4.2 Computational approach for the multi-objective design problem

Optimization (10) requires different risk metrics, $C(\mathbf{x})$, $C_{thresh}(\mathbf{x})$ and $F_{thresh}(\mathbf{x})$, whose estimation involves calculation of a probabilistic integral of the form (6). Stochastic simulation is adopted here for this estimation: using a finite number, N, of samples of $\boldsymbol{\theta}$ drawn from proposal density $q(\boldsymbol{\theta})$, an estimate for the risk integral of interest [expressed through generalized form of (6)] is:

$$\hat{H}_r(\mathbf{x}) = \frac{1}{N}\sum_{j=1}^{N} h_r(\mathbf{x},\boldsymbol{\theta}^j)\frac{p(\boldsymbol{\theta}^j)}{q(\boldsymbol{\theta}^j)} \quad , \tag{11}$$

where $\boldsymbol{\theta}^j$ denotes the sample used in the j^{th} simulation and $\{\boldsymbol{\theta}^j;\ j=1,\ldots,N\}$ represents the entire sample-set. The proposal density $q(\boldsymbol{\theta})$ is used to improve the efficiency of this estimation (i.e., reduce the coefficient of variation of that estimate), by focusing the computational effort on regions of the Θ space that contribute more to the integrand of the probabilistic integral in (6)- this corresponds to the concept of Importance Sampling (IS). Further details on IS implementation for seismic applications can be found in [22].

The design problem in (10) is solved by substituting the stochastic simulation estimates of form (11) for the required probabilistic integrals. The existence of the prediction error (stemming from the stochastic simulation) within the optimization is addressed by adopting an exterior sampling approach [30], utilizing the same, sufficiently large, number of samples throughout all iterations in the optimization process. That is, $\{\boldsymbol{\theta}^j;\ j=1,\ldots,N\}$ in (11) is chosen the same for each design configuration examined, therefore reducing the importance of the estimation error in the comparison of different design choices by creating a consistent error in these comparisons. Furthermore, for supporting an efficient optimization an approach relying on kriging surrogate modeling is adopted following the guidelines discussed in [29]. The surrogate model is established here to provide an approximate relationship between the design selection $\mathbf{x}$ (input to the surrogate model) and the risk quantities needed in the optimization (10), $C_{thresh}(\mathbf{x})$, $F_{thresh}(\mathbf{x})$, and $C_l(\mathbf{x})$ (outputs for the surrogate model) and is developed through the following approach. A large set of design configurations for the TMDI is first established to serve as support points for the kriging, utilizing a latin hypercube sampling in X. The response of each design configuration is then evaluated through time-history analysis, and then the risk quantities $C_{thresh}(\mathbf{x})$, $F_{thresh}(\mathbf{x})$, and $C_l(\mathbf{x})$ are calculated. Using this information the kriging metamodel is developed. This metamodel allows a highly efficient estimation of the risk measures of interest (thousands of evaluations within minutes) and is then used within the multi-objective optimization (10), coupled with an appropriate assumption for the upfront damper cost (used to calculate the overall cost C). The multi-objective problem can be then solved through any appropriate numerical method, for example through a blind-search approach or through genetic algorithms [31].

5. Case study

As case study the design of a TMDI for a 21-story existing building located in Santiago, Chile is considered [32]. The building has tapered elliptical shape, length 76.2 m and average depth 20 m (varying across its length), and has already a TMD installed in its last floor along its slender axis. The same configuration is examined here.

5.1 Model and cost characteristics

Seismic events occurrence are assumed to follow a Poisson distribution and so are history independent. The uncertainty in moment magnitude M is modeled by the Gutenberg-Richter relationship truncated on the interval $[M_{min}, M_{max}] = [5.5, 9.0]$, (events smaller than M_{min} do not contribute to the seismic risk) which leads to $p(M) = b_M e^{-b_M M} / (e^{-b_M M_{min}} - e^{-b_M M_{max}})$ and expected number of events per year $\nu = e^{a_M - b_M M_{min}} - e^{a_M - b_M M_{max}}$. The regional seismicity factors b_M and a_M are chosen by averaging the values for the seismic zones close to Santiago based on the recommendations in [33]. This results to $b_M = 0.8\log_e(10)$ and $a_M = 5.65\log_e(10)$. Regarding the uncertainty in the event location, the closest distance to the fault rupture, r_{rup}, for the earthquake events is assumed to follow a beta distribution in [30 250] km with median r_{med}=100 km and coefficient of variation 35%.

The linear structural model detailed in [18] is assumed for the considered primary structure. The total mass of the structure is 33.169.000 kg and Rayleigh damping is utilized by assigning an equal damping ratio for the first and second mode with 3% nominal value. The first three modes (and participation factors in parenthesis) are 2.10s (77%), 0.54s (16%) and 0.25s (5%). Pertinent data for the loss assessment model are reported in Table 1; lognormal fragility functions are adopted with median β_f and standard deviation σ_f for three different damageable assemblies: partitions, ceiling, and contents. For the first one, the *EDP* is taken as the peak inter-story drift and for the latter two as the peak floor acceleration. Note that damages to structural components are not included in this study since, as discussed earlier, they are expected to have small contribution (behavior remains elastic even for stronger events). The variable n_e in Table 1 corresponds to the number of elements per story whereas for each of the three different damageable assemblies different damage states are considered (total repair cost per assembly is obtained by considering the contribution from all damage states). The fragility function parameters for the partitions and the suspended ceiling are based on the recommendations in [34] whereas for the contents damageable subassembly the fragility curve used is similar to the one selected in [22].

Table 1 – Characteristics of fragility curves and expected repair cost and time for each story

Damage state	EDP	β_f	σ_f	n_{el} [++]	Repair cost (\$/n_{el})
		Partitions			
1(small cracks)	IDR[+]	0.21%	0.60	350 m^2	22.30
2(moderate cracks)	IDR	0.71%	0.45	350 m^2	60.30
3(severe damage)	IDR	1.2%	0.45	350 m^2	92.70
		Contents			
1(damage)	PFA[+]	0.70g	0.30	100	1000
		Ceiling			
1(some tiles fallen)	PFA	0.55g	0.40	1500 m^2	15.20
2(extensive tile fallout)	PFA	1.00g	0.40	1500 m^2	120.10
3(total ceiling collapse)	PFA	1.50g	0.40	1500 m^2	237.70

[+]IDR: Peak interstory drift; PFA: Peak floor acceleration
[++]n_{el}: number of elements per story

The discount rate is taken equal to 1.5% and the lifetime t_{life} is assumed to be 50 years. The repair cost and inerter force thresholds are taken to correspond to probability p_o=10% over t_{life}. The life-cycle cost and C_{thresh} for the uncontrolled structure are, respectively, \$2.02x10^6 and \$1.13x10^6 for the nominal structure (NS). The upfront TMDI cost is based on the attached mass. The underlying assumption is that the inerter and damper cost is by comparison negligible. This cost is approximated to be linearly related to the TMDI mass $C_i(\mathbf{x}) = b_c m$ [18] with value of b_c equal to 2500 \$/ton. This value is taken based on [35], additionally considering here that implementation is unidirectional and has no smart components (purely passive application).

5.3 Results and discussion

The design is performed here assuming a specific value of the inertance and optimizing over the remaining characteristics. This specific choice was made to better examine the impact of β on the optimal TMDI configurations. Therefore the design vector (corresponding also to the metamodel input is composed of the mass ratio μ, the damping ration ζ_d and the frequency ratio f_d. The analysis is performed for three different inertance ratios, β = 1, 5 and 10, whereas the ranges assumed for the design variables for developing the kriging metamodel are [0.1 1.0]% for μ (it is assumed that greater than 1.2% mass ratios are impractical to be achieved and ratios lower than 0.2% are too small for practical implementation), [0.01 0.8] for ζ_d and [0.3 1.5] for f_d. A total of 10,000 samples are used for the stochastic simulations to calculate the different risk metrics with importance sampling densities same as the ones discussed in [18]. This selection leads to coefficient of variation for the stochastic simulation below 6% for all metrics. Three different metamodels with 800 support points are therefore built, one for each β. The accuracy of the metamodels is high, with a coefficient of determination above 96% for most approximated response quantities. This accuracy level should be considered sufficient for performing optimization (10).

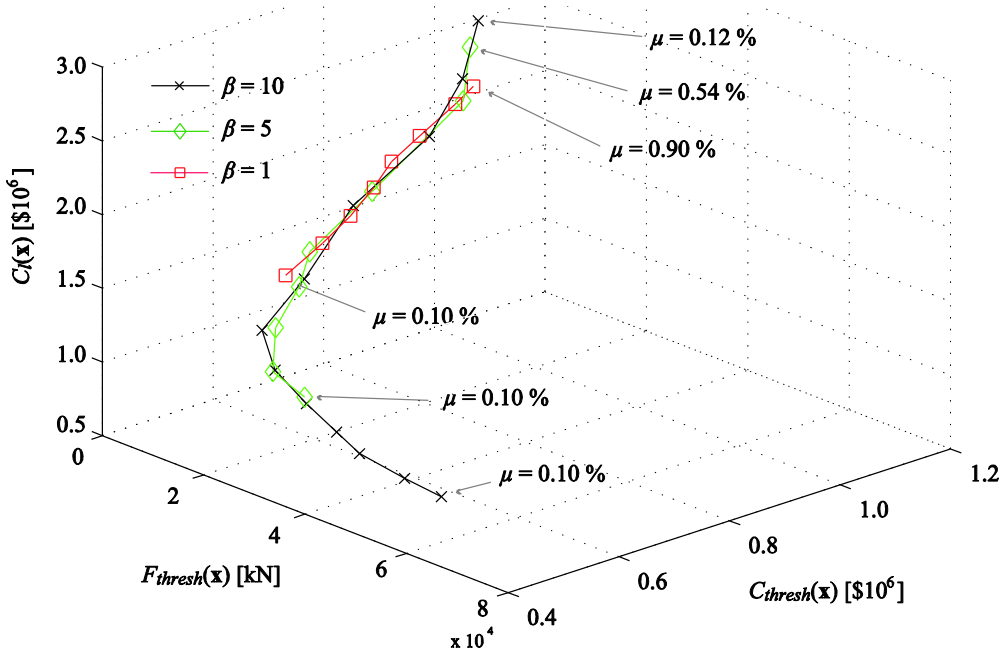

Fig. 3 – Pareto front in the three-objective space for different β values

Results from this optimization are presented in Figs. 3-5. Fig. 3 shows the pareto front for the three objectives [C_l(**x**)-C_{thresh}(**x**)-F_{thresh}(**x**)], for the three different β values. Fig. 4 then presents the projection of this front in the C_{thresh}(**x**)-F_{thresh}(**x**), the C_l(**x**)-F_{thresh}(**x**) and C_l(**x**)-C_{thresh}(**x**) planes. The mass ratio under optimal design is also shown for the extremes of the fronts, where it is possible to observe an increasing trend from one extreme to the other. The mass ratio is actually the main design variable changing across the front; the damping ratio and the frequency ratio simply take specific tuning values for that optimal mass ratio and follow the general trends for TMDIs reported in [13, 14]. This is the same trend observed in [18] when examining design of mass dampers based on life-cycle cost criteria [using combination of C_l(**x**) and C_{thresh}(**x**) objectives]. Optimal values for μ, ζ_d and f_d along the Pareto front [expressed as a function of objective C_{thresh}(**x**)] are reported in Fig. 5. The results show that the addition of the TMDI can provide a significant reduction for C_l(**x**) and C_{thresh}(**x**), with the benefits increasing, as expected, for larger inertance values. This validates the efficiency of the TMDI compared to the classical TMD as reported in the literature before [13, 14, 16, 17], this time in the context of seismic risk characterized through time-history analysis and adopting metrics related to life-cycle cost performance. This increase in protection efficiency comes, though, with a corresponding increase for the force that needs to be accommodated (larger F_{thresh}). In general, the results show that all three objectives are competing with one

another, demonstrating the value of the multi-objective problem (10) for exploring all candidate solutions that provide different compromises between the TMDI performance objectives.

Comparing the curves corresponding to different β values, it is immediately observable that larger β values lead to "wider" fronts, so greater potential variations across the objectives, with the fronts also overlapping in some ranges. This latter feature shows that similar performance can be achieved using different design configurations. The greatest improvement in terms of risk reduction (smaller values for $C_l(\mathbf{x})$ and $C_{thresh}(\mathbf{x})$) corresponds to larger β and lower μ at the expense, though, of large inerter forces as discussed earlier. Note also that a plateau is reached for the seismic risk with respect to the $F_{thresh}(\mathbf{x})$ objective; beyond certain value for F_{thresh} (different for each β case) small benefits are obtained for $C_l(\mathbf{x})$ and $C_{thresh}(\mathbf{x})$ for significant increase of $F_{threshi}$. This feature, which is common in multi-objective design problems (i.e. large deterioration of one objective for small only benefits for the competing objectives), should be carefully evaluated when making final design decisions. Finally, note that many of the identified solutions yield a larger value for $C_l(\mathbf{x})$ compared to the uncontrolled structure. These solutions, corresponding generally to large mass ratios, contribute, though, to significant reduction in $C_{thresh}(\mathbf{x})$ with small $F_{thresh}(\mathbf{x})$ demands. From a risk-aversion perspective such solutions could be ultimately preferred (reduction of effect of rare but high-consequence events), especially since they can be promoted with a reduced strengthening of the structural frame, sufficient to accommodate the relatively smaller inerter forces.

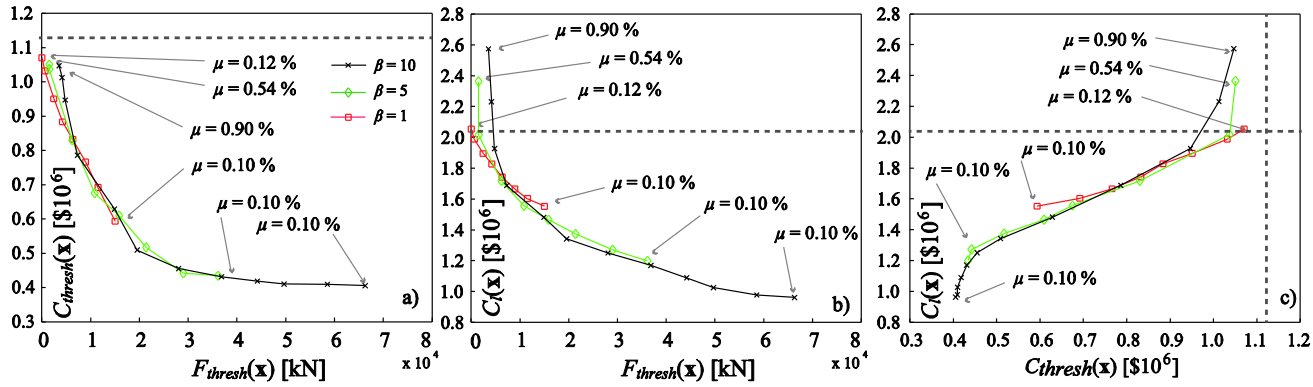

Fig. 4 – Projection of the Pareto front along pair of objectives (each case presented for different β values). Dashed lines correspond to the performance of the structure without the TMDI.

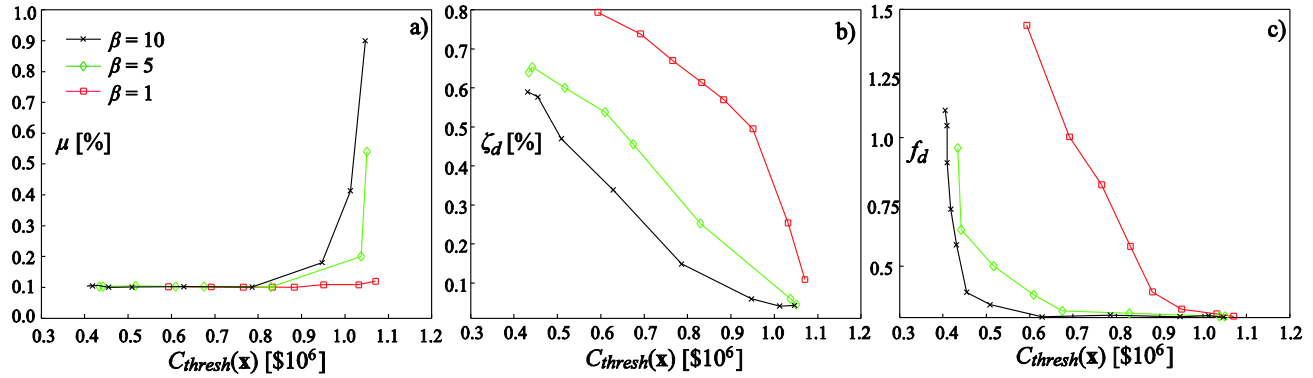

Fig. 5 – Optimal values for μ, ζ_d and f_d along the Pareto front [design variables are plotted with respect to the corresponding value of $C_{thresh}(\mathbf{x})$].

6. Conclusions

A risk-informed design procedure of TMDIs for seismic protection of multi-story buildings in the region of Chile was presented. The seismic hazard was described by a stochastic ground motion model that was calibrated to offer compatibility with the ground motion predictive equation available for Chile. Three different criteria

were utilized in the design optimization. The first one, representing the direct benefits from the damper implementation, is the life-cycle cost of the system, composed by the TMDI upfront cost and the anticipated seismic losses over the lifetime of the structure. The upfront cost was related only to the TMDI mass while the seismic losses were identified by adopting a vulnerability approach using the time-history response of the structure under the hazard provided by the ground motion model. The two additional criteria corresponded to the repair cost and the inerter force associated to a specific probability of exceedance over the structure lifetime. The repair cost incorporates risk-averse attitudes while the inerter force expresses practical constraints for the force transmitted from the TMDI to the structure. A multi-objective optimization was established considering these three objectives while stochastic simulation techniques were used to obtain all risk measures. Additionally, a Kriging metamodel was developed to support an efficient optimization process. A case study was presented employing a specific 21-story building located in Santiago, Chile. The results showed that the proposed design framework facilitates a clear demonstration of the benefits of the TMDI over the TMD as well as the evaluation of the comparative benefits of increasing the TMD mass vis-a-vis increasing the inertance of the TMDI. The greatest improvement in terms of risk reduction corresponds to larger inertance and lower mass at the expense of accommodating larger inerter forces. Configurations corresponding to large masses yield higher total life-cycle cost compared to the uncontrolled structure, but at the same time contribute to significant reduction in repair cost threshold for rare events with reduced inerter forces to accommodate. From a risk-aversion perspective such solutions may be preferred, especially since they can be promoted with a reduced local strengthening.

7. Acknowledgements

The second author gratefully acknowledges the support of EPSRC, UK under grant EP/M017621/1. The dynamic properties of the structure considered in the case study described in Section 5 were provided by VMB Ingenieria Estructural (Santiago, Chile).

8. References

[1] Kareem A, Kline S (1993) Performance of multiple mass dampers under random loading. *Journal of Structural engineering, ASCE*, **121** (2), 348-361.

[2] Soto MG, Adeli H (2013) Tuned mass dampers. *Archives of Computational Methods in Engineering*, **20** (4), 419-431.

[3] Chang CC (1999) Mass dampers and their optimal designs for building vibration control *Engineering Structures*, **21**, 454-463.

[4] Rana R, Soong TT (1998) Parametric study and simplified design of tuned mass dampers. *Engineering Structures*, **20** (3), 193-204.

[5] Den Hartog JP (1947) *Mechanical Vibrations*. New York, NY: McGraw-Hill, Inc.

[6] Tigli OF (2012) Optimum vibration absorber (tuned mass damper) design for linear damped systems subjected to random loads. *Journal of sound and vibration*, **331** (13), 3035-3049.

[7] De Angelis M, Perno S, Reggio A (2012) Dynamic response and optimal design of structures with large mass ratio TMD. *Earthquake Engineering & Structural Dynamics*, **41** (1), 41-60.

[8] Hoang N, Fujino Y, Warnitchai P (2008) Optimal tuned mass damper for seismic applications and practical design formulas. *Engineering Structures*, **30** (3), 707-715.

[9] Matta E (2011) Performance of tuned mass dampers against near-field earthquakes. *Structural Engineering and Mechanics*, **39** (5), 621-642.

[10] Matta E, De Stefano A (2009) Seismic performance of pendulum and translational roof-garden TMDs. *Mechanical Systems and Signal Processing*, **23** (3), 908-921.

[11] Matta E, De Stefano A (2009) Robust design of mass-uncertain rolling-pendulum TMDs for the seismic protection of buildings. *Mechanical Systems and Signal Processing*, **23** (1), 127-147.

[12] Feng MQ, Mita A (1995) Vibration control of tall buildings using mega subconfiguration. *Journal of Engineering Mechanics*, **121** (10), 1082-1088.

[13] Marian L, Giaralis A (2013) Optimal design of inerter devices combined with TMDs for vibration control of buildings exposed to stochastic seismic excitations. *11th International Conference on Structural Safety and Reliability*, June 16-20 New York, US.

[14] Marian L, Giaralis A (2014) Optimal design of a novel tuned mass-damper-inerter (TMDI) passive vibration control configuration for stochastically support-excited structural systems. *Probabilistic Engineering Mechanics*, **38**, 156-164.

[15] Smith MC (2002) Synthesis of mechanical networks: the inerter. *Automatic Control, IEEE Transactions on*, **47** (10), 1648-1662.

[16] Giaralis A, Taflanidis AA (2015) Reliability-based design of tuned mass-damper-inerter (TMDI) equipped multi-storey frame buildings under seismic excitation. *12th International Conference on Applications of Statistics and Probability in Civil Engineering*, July 12-15 Vancouver, Canada.

[17] Giaralis A, Marian L (2016) Use of inerter devices for weight reduction of tuned mass-dampers for seismic protection of multi-story building: the Tuned Mass-Damper-Interter (TMDI). *SPIE 9799, Active and Passive Smart Structures and Integrated Systems* 20-24 March Las Vegas, Nevada.

[18] Ruiz R, Taflanidis AA, Lopez-Garcia D, Vetter C (2015) Life-cycle based design of mass dampers for the Chilean region and its application for the evaluation of the effectiveness of tuned liquid dampers with floating roof. *Bulletin of Earthquake Engineering*, **14** (3), 943-970.

[19] Papageorgiou C, Smith MC (2005) Laboratory experimental testing of inerters. *Decision and Control, 2005 and 2005 European Control Conference. CDC-ECC'05. 44th IEEE Conference*.

[20] Wang F-C, Hong M-F, Lin T-C (2011) Designing and testing a hydraulic inerter. *Proceedings of the Institution of Mechanical Engineers, Part C: Journal of Mechanical Engineering Science*, **225** (1), 66-72.

[21] Swift SJ, Smith MC, Glover AR, Papageorgiou C, Gartner B, Houghton NE (2013) Design and modelling of a fluid inerter. *International Journal of Control*, **86** (11), 2035-2051.

[22] Taflanidis AA, Beck JL (2009) Life-cycle cost optimal design of passive dissipative devices. *Structural Safety*, **31** (6), 508-522.

[23] Porter KA, Kiremidjian AS, LeGrue JS (2001) Assembly-based vulnerability of buildings and its use in performance evaluation. *Earthquake Spectra*, **18** (2), 291-312.

[24] Vetter C, Taflanidis AA, Mavroeidis GP (2016) Tuning of stochastic ground motion models for compatibility with ground motion prediction equations. *Earthquake Engineering and Structural Dynamics*, **45** (6), 893-912.

[25] Boroschek R, Contreras V (2012) Strong ground motion form the 2010 Mw 8.8 Maule Chile earthquake and attenuation relations for Chilean subduction zone interface earthquakes. *International Symposium on Engineering Lessons Learned from the 2011 Great East Japan earthquake*, March 1-4 Tokyo, Japan.

[26] Jalayer F, Beck JL (2008) Effects of two alternative representations of ground-motion uncertainty in probabilistic seismic demand assessment of structures. *Earthquake Engineering and Structural Dynamics*, **37** (1), 61-79.

[27] Goulet CA, Haselton CB, Mitrani-Reiser J, Beck JL, Deierlein G, Porter KA, Stewart JP (2007) Evaluation of the seismic performance of code-conforming reinforced-concrete frame building-From seismic hazard to collapse safety and economic losses. *Earthquake Engineering and Structural Dynamics*, **36** (13), 1973-1997.

[28] Gidaris I, Taflanidis AA, Mavroeidis GP (2014): Multi-objective design of fluid viscous dampers using life-cycle cost criteria. *10th National Conference in Earthquake Engineering* Anchorage, AK.

[29] Gidaris I, Taflanidis AA (2015) Performance assessment and optimization of fluid viscous dampers through life-cycle cost criteria and comparison to alternative design approaches. *Bulletin of Earthquake Engineering*, **13** (4), 1003-1028.

[30] Spall JC (2003): *Introduction to stochastic search and optimization*. New York: Wiley-Interscience.

[31] Coello CAC, Van Veldhuizen DA, Lamont GB (2002) *Evolutionary algorithms for solving multi-objective problems* (Vol. 242): Springer.

[32] Zemp R, de la Llera JC, Roschke P (2011) Tall building vibration control using a TM-MR damper assembly: Experimental results and implementation. *Earthquake Engineering & Structural Dynamics*, **40** (3), 257-271.

[33] Leyton F, Ruiz S, Sepulveda SA (2009) Preliminary re-evaluation of probabilistic seismic hazard assessment in Chile: from Arica to Taitao Peninsula. *Advances in Geosciences*, **22** (22), 147-153.

[34] FEMA-P-58 (2012) *Seismic performance assessment of buildings*. Redwood City, CA. American Technology Council.

[35] Tse KT, Kwok KCS, Tamura Y (2012) Performance and cost evaluation of a smart tuned mass damper for suppressing wind-induced lateral-torsional motion of tall structures. *Journal of Structural Engineering*, **138** (4), 514-525.